Inorg. Chem. **2004**, *43*, 651–662

Synthesis and Spectroscopy of μ-Oxo (O^{2-})-Bridged Heme/Non-heme Diiron Complexes: Models for the Active Site of Nitric Oxide Reductase

Ian M. Wasser,[†] Constantinus F. Martens,[†] Claudio N. Verani,[†,‡] Eva Rentschler,[§] Hong-wei Huang,[||] Pierre Moënne-Loccoz,[||] Lev N. Zakharov,[⊥,▽] Arnold L. Rheingold,[⊥,▽] and Kenneth D. Karlin*[,†]

Department of Chemistry, Johns Hopkins University, Charles and 34th Streets, Baltimore, Maryland 21218, Max-Planck Institut für Strahlenchemie, Stiftstrasse 34-36, 45470 Mülheim an der Ruhr, Germany, Department of Environmental and Biomolecular Systems, OGI School of Science and Engineering at the Oregon Health & Science University (OHSU), Beaverton, Oregon 97006, and Department of Chemistry, University of Delaware, Newark, Delaware 19716

Received July 12, 2003

In this paper, we describe the synthesis and study of a series of heme/non-heme Fe–O–Fe′ complexes supported by a porphyrin and the tripodal nitrogen ligand TMPA [TMPA = tris(2-pyridylmethyl)amine]. The complete synthesis of $[(^6L)Fe–O–Fe(X)]^+$ (**1**) (X = OMe^- or Cl^-, 69:31 ratio), where ^6L is the dianion of 5-(*o*-*O*-[(*N*,*N*-bis(2-pyridylmethyl)-2-(6-methoxyl)pyridinemethanamine)phenyl]-10,15,20-tris(2,6-difluorophenyl)porphine, is reported. The crystal structure for **1**·PF_6 reveals an intramolecular heme/non-heme diferric complex bridged by an Fe–O–Fe′ moiety; ∠(Fe–O–Fe′) = 166.7(3)°, and *d*(Fe···Fe′) = 3.556 Å. Crystal data for $C_{70}H_{57}ClF_{12}Fe_2N_8O_3P$ (**1**·PF_6): triclinic, $P\bar{1}$, *a* = 13.185(3) Å, *b* = 14.590 (3) Å, *c* = 16.885(4) Å, α = 104.219(4)°, β = 91.572(4)°, γ = 107.907(4)°, *V* = 2977.3(11) Å^3, *Z* = 2, *T* = 150(2) K. Complex **1** (where X = Cl^-) is further characterized by UV–vis (λ_{max} = 328, 416 (Soret), 569 nm), ^{1}H NMR (δ 27–24 [TMPA –CH_2–], 16.1 [pyrrole-H], 15.2–10.5 [PY-3H, PY-5H], 7.9–7.2 [*m*- and *p*-phenyl-H], 6.9–5.8 [PY-4H] ppm), resonance Raman (ν_{as}(Fe–O–Fe′) 844 cm^{-1}), and Mössbauer (δ_{Fe} = 0.47, 0.41 mm/s; ΔE_A = 1.59, 0.55 mm/s; 80 K) spectroscopies, MALDI-TOF mass spectrometry (*m*/*z* 1202), and SQUID susceptometry (*J* = – 114.82 cm^{-1}, *S* = 0). We have also synthesized a series of 3-, 4-, and 5-methyl-substituted as well as selectively deuterated TMPA(Fe′) complexes and condensed these with the hydroxo complex (F_8)FeOH or (F_8-d_8)FeOH to yield "untethered" Fe–O–Fe′ analogues. Along with selective deuteration of the methylene hydrogens in TMPA, complete ^{1}H NMR spectroscopic assignments for **1** have been accomplished. The magnetic properties of several of the untethered complexes and a comparison to those of **1** are also presented. Complex **1** and related species represent good structural and spectroscopic models for the heme/non-heme diiron active site in the enzyme nitric oxide reductase.

Introduction

The inorganic nitrogen cycle controls the fate of many pollutants, including nitrate (a water pollutant), as well as the tropospheric pollutants known as NO_x, mainly nitric oxide (NO) and nitrous oxide (N_2O).[1] In the denitrification cycle, an alternative to aerobic respiration or photosynthesis, *N*-oxides are utilized as terminal electron acceptors, driving the reduction of nitrate to dinitrogen:[1−6]

$$NO_3^- \rightarrow NO_2^- \rightarrow NO \rightarrow N_2O \rightarrow N_2$$

The overall five-electron reduction takes place in four steps, catalyzed at each step by one (or more) metalloen-

* Author to whom correspondence should be addressed. E-mail: karlin@jhu.edu.
† Johns Hopkins University.
‡ Current address: Department of Chemistry, Wayne State University, 5101 Cass Ave., Detroit, MI 48202.
§ Max-Planck Institut für Strahlenchemie.
|| OGI School of Science and Engineering at the OHSU.
⊥ University of Delaware.
▽ Current address: Department of Chemistry and Biochemistry, University of California at San Diego, 9500 Gilman Dr., La Jolla, CA 92093.

(1) Zumft, W. G. *Microbiol. Mol. Biol. Rev.* **1997**, *61*, 533−616.
(2) Moura, I.; Moura, J. J. G. *Curr. Opin. Chem. Biol.* **2001**, *5*, 168−175.
(3) Averill, B. A. *Chem. Rev.* **1996**, *96*, 2951−2964.
(4) Berks, B. C.; Ferguson, S. J.; Moir, J. W.; Richardson, D. J. *Biochim. Biophys. Acta* **1995**, *1232*, 97−173.
(5) Wasser, I. M.; de Vries, S.; Moënne-Loccoz, P.; Schröeder, I.; Karlin, K. D. *Chem. Rev.* **2002**, *102*, 1201−1234.

10.1021/ic0348143 CCC: $27.50
Published on Web 12/13/2003

zyme(s): Nitrate reductase (NAR) employs a molybdenum oxotransferase species to accomplish the two-electron reduction of nitrate to nitrite. Nitrite reductase (NIR), which facilitates the one-electron reduction of nitrite to nitric oxide, utilizes either a heme cd_1 or a copper active site.[7,8] The final reduction of nitrous oxide to dinitrogen is accomplished by nitrous oxide reductase (N_2OR), a multicopper enzyme with a $Cu_4(S)$ core.[9−11] The middle enzyme, nitric oxide reductase (NOR), contains a μ-oxo-bridged heme/non-heme moiety in the oxidized active site.[12−14] A close analogy between the active sites of NOR and cytochrome *c* oxidase (C*c*O) has been suggested; C*c*O and NOR are genetic cousins.[1,5]

Our own interest in this area stems from the examination of heme/copper oxidase model complexes and their interactions with dioxygen, relevant to the heme a_3/Cu_B active site in cytochrome *c* oxidase.[15−18] The iron/copper systems employ a binucleating ligand featuring a porphyrin tethered to a tetradentate chelate (tris(2-pyridylmethyl)amine, TMPA) able to coordinate copper. A natural extension of this system consists of employing the same ligand framework, substituting an iron ion for copper in the TMPA. Such an approach has been previously reported with the complex [(^{5}L)Fe−O−Fe(Cl)](ClO_4) (**2**·ClO_4), where ^{5}L is the dianion of 5-(*o*-*O*-[(*N*,*N*-bis(2-pyridylmethyl)-2-(5-methoxyl)pyridinemethanamine)phenyl]-10,15,20-tris(2,6-difluorophenyl)porphine.[14,19,20]

The μ-oxo (O^{2-}) diferric unit has been studied extensively,[21] with much interest stemming from its magnetic coupling and occurrence in the active sites of many metalloproteins.[21−25] Synthetic Fe−O−Fe′ complexes, also bridged by carboxylates, have been employed to model the structural features and dioxygen reactivity observed in such biological systems as hemerythrin,[26−34] ribonucleotide reductase and methane monooxygenase.[26,29,33,35−40]

Here, we report the synthesis and spectroscopic characterization of several related new heme/non-heme diiron complexes, both tethered and untethered systems, representing spectroscopic models for the putative resting (oxidized) site in NOR. The synthesis, X-ray structure, magnetochemical measurements, and Mössbauer, resonance Raman, and ^{1}H NMR spectroscopies are presented for [(^{6}L)Fe−O−Fe(Cl)]$B(C_6F_5)_4$ (**1**·BArF) and [(^{6}L)Fe−O−Fe(Cl)]PF_6 (**1**·PF_6). Additional synthetic procedures, along with magnetic and Mössbauer data, are also presented for the related complexes [(F_8)Fe−O−Fe(Cl)(TMPA)]ClO_4 (**3**·ClO_4) and [(F_8)Fe−O−Fe(Cl)(3-Me$_3$TMPA)]ClO_4 (**6**·ClO_4) (F_8 = the dianion of tetrakis(2,6-difluorophenyl)porphyrinate, 3-Me$_3$TMPA = tris-(3-methyl-2-pyridylmethyl)amine). Furthermore, we present thorough ^{1}H NMR assignments for **1**−**3**, obtained by examining a series (**4**−**8**) of methyl- and deuterium-substituted, Fe−O−Fe′ analogues. Figure 1 shows the structures for the compounds used in this study, **1**−**8**.

Experimental Section

Materials and Methods. Reagents were obtained from commercial sources. Dichloromethane (CH_2Cl_2) was purified by passing reagent-grade solvent through an activated alumina column. Acetone was distilled from nonindicating anhydrous calcium sulfate. Acetonitrile, methanol, heptane, and pentane were predried and distilled over CaH_2. Tetrahydrofuran (THF) was predried over KOH before

(6) Richardson, D. J.; Watmough, N. J. *Curr. Opin. Chem. Biol.* **1999**, *3*, 207−219.
(7) Godden, J. W.; Turley, S.; Teller, D. C.; Adman, E. T.; Liu, M. Y.; Payne, W. J.; LeGall, J. *Science* **1991**, *253*, 438−442.
(8) Murphy, M. E. P. T., S.; Kukimoto, M.; Nishiyama, M.; Horinouchi, S.; Sasaki, H.; Tanokura, M.; Adman, E. T. *Biochemistry* **1995**, *34*, 12107−12117.
(9) Brown, K.; Djinovic-Carugo, K.; Haltia, T.; Cabrito, I.; Saraste, M.; Moura, J. J. G.; Moura, I.; Tegoni, M.; Cambillau, C. *J. Biol. Chem.* **2000**, *275*, 41133−41136.
(10) Rasmussen, T. B., B. C.; Sanders-Loehr, J.; Dooley, D. M.; Zumft, W. G.; Thomson, A. J. *Biochemistry* **2000**, *39*, 12753−12756.
(11) Alvarez, M. L.; Ai, J.; Zumft, W.; Sanders-Loehr, J.; Dooley, D. M. *J. Am. Chem. Soc.* **2001**, *123*, 576−587.
(12) Girsch, P.; de Vries, S. *Biochim. Biophys. Acta* **1997**, *1318*, 202−216.
(13) Moënne-Loccoz, P.; de Vries, S. *J. Am. Chem. Soc.* **1998**, *120*, 5147−5152.
(14) Moënne-Loccoz, P.; Richter, O.-M. H.; Huang, H.-W.; Wasser, I. M.; Ghiladi, R. A.; Karlin, K. D.; de Vries, S. *J. Am. Chem. Soc.* **2000**, *122*, 9344−9345.
(15) Ghiladi, R. A.; Ju, T. D.; Lee, D.-H.; Moënne-Loccoz, P.; Kaderli, S.; Neuhold, Y.-M.; Zuberbüehler, A. D.; Woods, A. S.; Cotter, R. J.; Karlin, K. D. *J. Am. Chem. Soc.* **1999**, *121*, 9885−9886.
(16) Ju, T. D.; Ghiladi, R. A.; Lee, D.-H.; van Strijdonck, G. P. F.; Woods, A. S.; Cotter, R. J.; Young, V. G., Jr.; Karlin, K. D. *Inorg. Chem.* **1999**, *38*, 2244−2245.
(17) Obias, H. V.; van Strijdonck, G. P. F.; Lee, D.-H.; Ralle, M.; Blackburn, N. J.; Karlin, K. D. *J. Am. Chem. Soc.* **1998**, *120*, 9696−9697.
(18) Kim, E.; Helton, M. E.; Wasser, I. M.; Karlin, K. D.; Lu, S.; Huang, H.-W.; Moënne-Loccoz, P.; Incarvito, C. D.; Rheingold, A., L.; Honecker, M.; Kaderli, S.; Zuberbuhler, A. D. *Proc. Natl. Acad. Sci. U.S.A.* **2003**, *100*, 3623−3628.
(19) Martens, C. F.; Murthy, N. N.; Obias, H. V.; Karlin, K. D. *J. Chem. Soc., Chem. Commun.* **1996**, 629−630.
(20) Ju, T. D.; Woods, A. S.; Cotter, R. J.; Moënne-Loccoz, P.; Karlin, K. D. *Inorg. Chim. Acta* **2000**, *297*, 362−372.
(21) Kurtz, J., D. M. *Chem. Rev.* **1990**, *90*, 585−606.
(22) Vincent, J. B.; Olivier-Lilly, G. L.; Averill, B. A. *Chem. Rev.* **1990**, *90*, 1447−1467.
(23) Wallar, B. J.; Lipscomb, J. D. *Chem. Rev.* **1996**, *96*, 2625−2657.
(24) Feig, A. L.; Lippard, S. J. *Chem. Rev.* **1994**, *94*, 759−805.
(25) Lippard, S. J. *Angew. Chem.* **1988**, *100*, 353−371.
(26) Zang, Y.; Pan, G.; Que, L., Jr.; Fox, B. G.; Münck, E. *J. Am. Chem. Soc.* **1994**, *116*, 3653−3654.
(27) Mizoguchi, T. J.; Kuzelka, J.; Spingler, B.; DuBois, J. L.; Davydov, R. M.; Hedman, B.; Hodgson, K. O.; Lippard, S. J. *Inorg. Chem.* **2001**, *40*, 4662−4673.
(28) He, C.; Barrios, A. M.; Lee, D.; Kuzelka, J.; Davydov, R. M.; Lippard, S. J. *J. Am. Chem. Soc.* **2000**, *122*, 12683−12690.
(29) Payne, S. C.; Hagen, K. S. *J. Am. Chem. Soc.* **2000**, *122*, 6399−6410.
(30) Mimmi, M. C.; Micciche, F.; Kooijman, H.; Spek, A. L.; Warzeska, S. T.; Bouwman, E. *Inorg. Chim. Acta* **2002**, *340*, 197−200.
(31) Norman, R. E.; Holz, R. C.; Menage, S.; Que, L., Jr.; Zhang, J. H.; O'Connor, C. J. *Inorg. Chem.* **1990**, *29*, 4629−4637.
(32) Norman, R. E.; Yan, S.; Que, L., Jr.; Backes, G.; Ling, J.; Sanders-Loehr, J.; Zhang, J. H.; O'Connor, C. J. *J. Am. Chem. Soc.* **1990**, *112*, 1554−1562.
(33) Mizoguchi, T. J.; Davydov, R. M.; Lippard, S. J. *Inorg. Chem.* **1999**, *38*, 4098−4103.
(34) Mizoguchi, T. J.; Lippard, S. J. *J. Am. Chem. Soc.* **1998**, *120*, 11022−11023.
(35) Lee, D.; Pierce, B.; Krebs, C.; Hendrich, M. P.; Huynh, B. H.; Lippard, S. J. *J. Am. Chem. Soc.* **2002**, *124*, 3993−4007.
(36) Dong, Y.; Fujii, H.; Hendrich, M. P.; Leising, R. A.; Pan, G.; Randall, C. R.; Wilkinson, E. C.; Zang, Y.; Que, L., Jr.; Fox, B. G.; Kauffmann, K.; Münck, E. *J. Am. Chem. Soc.* **1995**, *117*, 2778−2792.
(37) Zheng, H.; Zang, Y.; Dong, Y.; Young, V. G., Jr.; Que, L., Jr. *J. Am. Chem. Soc.* **1999**, *121*, 2226−2235.
(38) Lee, D.; Lippard, S. J. *J. Am. Chem. Soc.* **1998**, *120*, 12153−12154.
(39) Hagadorn, J. R.; Que, L., Jr.; Tolman, W. B. *J. Am. Chem. Soc.* **1998**, *120*, 13531−13532.
(40) Nivorozhkin, A. L.; Anxolabehere-Mallart, E.; Mialane, P.; Davydov, R.; Guilhem, J.; Cesario, M.; Schussler, L.; Audiere, J.-P.; Girerd, J.-J.; Styring, S.; Seris, J.-L. *Inorg. Chem.* **1997**, *36*, 846−853.

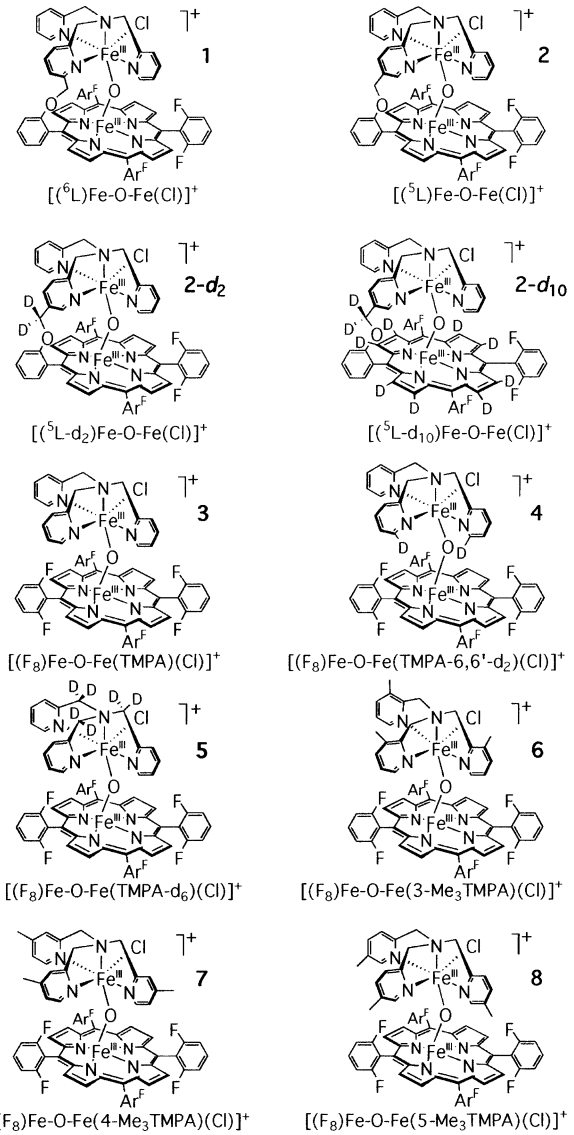

Figure 1. Synthetic Fe−O−Fe′ heme/non-heme diiron complexes studied.

being distilled over Na/benzophenone ketyl. The preparation and handling of air-sensitive materials was carried out with Schlenk techniques under argon or in an MBraun Labmaster 130 glovebox under nitrogen. Elemental analyses were performed by Desert Analytics, Tucson, AZ, National Chemical Consulting Inc., Tenafly, NJ, or Quantitative Technologies, Inc. (QTI), Whitehouse, NJ. ^{1}H NMR spectra were recorded at 300 MHz on a Bruker AMX-300 instrument. ^{2}H NMR spectra were collected at 61 MHz on a Varian NMR instrument. Chemical shifts are reported as δ values, downfield from that of an internal standard (Me_4Si) or the residual solvent proton peak (for ^{1}H NMR). All ^{2}H NMR spectra were recorded in $CHCl_3$ with 2 μL of $CDCl_3$ added as an internal reference. Infrared spectra were obtained on either a Mattson Galaxy 4030 FT-IR spectrometer or an ASI ReactIR 1000 FTIR spectrometer with a SiComp ATR probe tip. Solid samples were prepared as KBr pellets or by allowing concentrated solutions of a sample to evaporate onto the SiComp ATR probe window. UV−vis spectra were recorded on a Shimadzu UV 160 spectrometer or a Perkin-Elmer Lamba Array 3840. Fast-atom bombardment mass spectrometry (FAB-MS) and electrospray ionization mass spectrometry (ESI-MS) were performed by the Mass Spectrometry Facility at Johns Hopkins University. Matrix-assisted laser desorption−ionization time-of-flight mass spectrometry (MALDI-TOF-MS) was performed using a Kratos Kompact 4 spectrometer, and the porphyrin complexes were examined without added matrix.

Warning: Although we have experienced no difficulties with the perchlorate complexes described herein, these compounds should be regarded as potentially explosive and handled accordingly!

Synthesis. The complexes (F_8)FeOH,[41] $(F_8$-$d_8)$FeOH,[41] $(F_6$-d_8-$H_2)$OH,[42] (^5L)FeOH,[17] $(^6L)Fe^{II}$ "empty tether",[16] TMPA,[43] TMPA-*6,6′-d*$_2$,[44] TMPA-d_6,[44] 3-Me_3TMPA,[44] 4-Me_3TMPA,[44] 5-Me_3TMPA,[36,44] (TMPA)CD_2Cl,[17] and $[(^5L$-$d_2)$Fe−O−Fe(Cl)]ClO_4,[17] were prepared following literature procedures.

^{5}L-d_{10}. A procedure, analogous to that employed for the synthesis of ^{5}L was followed,[17] condensing (TMPA)CD_2Cl and $(F_6$-d_8-$H_2)$-OH in acetone using an excess of K_2CO_3. ^{2}H NMR ($CHCl_3$, 61 MHz): δ 8.87 (pyrrole-D), 4.94 (CD_2O).

[(L)FeCl$_2$]ClO$_4$ (L = TMPA, TMPA-6,6′-*d*$_2$, TMPA-*d*$_6$, 3-Me$_3$TMPA, 4-Me$_3$TMPA, 5-Me$_3$TMPA). The various complexes were all prepared in the same manner. A general procedure is as follows: to a 50 mL round-bottom flask containing a solution of L (1.8 mmol) dissolved in 10 mL of MeOH is added $FeCl_3 \cdot 6H_2O$ (485 mg, 1.8 mmol) as a solid. The mixture turns yellow-brown and is stirred for 30 min. Then $(Bu)_4NClO_4$ (1.22 g, 3.6 mmol), dissolved in 1 mL of MeOH, is added. In most cases this results in the immediate precipitation of the desired mononuclear $[(L)FeCl_2]ClO_4$ complex, all as bright-yellow microcrystalline solids. A small amount of the μ-oxo (O^{2-}) "dimer" $\{[(L)FeCl]_2O\}(ClO_4)_2$ is sometimes formed, precipitating immediately as a brown powder that can be filtered off. Cooling of the remaining supernatant results in precipitation of the mononuclear $[(L)FeCl_2]ClO_4$ complexes.

Data for L = TMPA. ^{1}H NMR (CD_3CN, 300 MHz): δ 162 (br), 118, 111, 97. FTIR (KBr, cm^{-1}): 2976, 1607, 1483, 1441, 1292, 1082, 781, 623. FAB-MS (*m*-nitrobenzyl alcohol matrix): *m*/*z* 416 $(M - ClO_4^-)^+$.

Data for L = TMPA-6,6′-*d*$_2$. ^{1}H NMR (CD_3CN, 300 MHz): δ 160, 136, 112, 98. ^{2}H NMR (CH_3CN, 300 MHz): pyridine 6-D not detected. FTIR (KBr, cm^{-1}): 2979, 2934, 1600, 1445, 1095, 1024, 906, 829, 780, 624. FAB-MS (*m*-nitrobenzyl alcohol matrix): *m*/*z* 418 $(M - ClO_4^-)^+$.

Data for L = TMPA-*d*$_6$. ^{1}H NMR (CD_3CN, 300 MHz): δ 138, 114, 99. ^{2}H NMR (CD_3CN, 300 MHz): δ 165. FTIR (KBr, cm^{-1}): 3109, 3032, 1609, 1566, 1483, 1445, 1300, 1263, 1094, 910, 826, 777, 712, 652, 623, 486, 426. FAB-MS (*m*-nitrobenzyl alcohol matrix): *m*/*z* 422 $(M - ClO_4^-)^+$.

Data for L = 3-Me$_3$TMPA. ^{1}H NMR (CD_3CN, 300 MHz): δ 156 (br), 143, 121, 6.84, 4.83, −0.05. FTIR (KBr, cm^{-1}): 3094, 2965, 2932, 1595, 1449, 1389, 1238, 1182, 1103, 1078, 1007, 951, 907, 799, 714, 623. FAB-MS (*m*-nitrobenzyl alcohol matrix): *m*/*z* 458 $(M - ClO_4^-)^+$.

Data for L = 4-Me$_3$TMPA. FTIR (KBr, cm^{-1}): 2963, 1620, 1561, 1487, 1445, 1346, 1290, 1105, 1082, 1026, 914, 835, 623.

Data for L = 5-Me$_3$TMPA. FTIR (KBr, cm^{-1}): 3055, 2963, 2928, 2878, 1615, 1578, 1501, 1454, 1408, 1294, 1221, 2076, 903, 826, 725, 664, 623.

(41) Karlin, K. D.; Nanthakumar, A.; Fox, S.; Murthy, N. N.; Ravi, N.; Huynh, B. H.; Orosz, R. D.; Day, E. P. *J. Am. Chem. Soc.* **1994**, *116*, 4753−4763.
(42) Ghiladi, R. A.; Karlin, K. D. *Inorg. Chem.* **2002**, *41*, 2400−2407.
(43) Tyeklár, Z.; Jacobson, R. R.; Wei, N.; Murthy, N. N.; Zubieta, J.; Karlin, K. D. *J. Am. Chem. Soc.* **1993**, *115*, 2677−2689.
(44) Nanthakumar, A.; Fox, S.; Murthy, N. N.; Karlin, K. D. *J. Am. Chem. Soc.* **1997**, *119*, 3898−3906.

[(^{6}L)Fe−O−Fe(Cl)]B(C_6F_5)$_4$ (1·BArF). In a 100 mL airless flask, charged with a stirbar, were mixed 250 mg (0.228 mmol) of (^{6}L)Fe^{II} empty tether, 29 mg (0.23 mmol) of $FeCl_2$, and 175 mg (0.23 mmol) of lithium tetrakis(pentafluorophenyl)borate etherate. The solids were dissolved in 10 mL of tetrahydrofuran and stirred under argon for 20 min and then subsequently stirred in the ambient atmosphere for 4 h. Tetrahyrdrofuran was evaporated under reduced pressure, and the resulting red-brown solid was redissolved in 150 mL of methylene chloride and transferred to a separatory funnel. The organic layer was washed with aqueous sodium chloride (1 × 200 mL) and then washed with distilled water (2 × 200 mL). The organic layer was isolated, dried over sodium sulfate, and recrystallized at −20 °C from methylene chloride and heptane. The recrystallized solid was washed with pentane (3 × 50 mL) until the washings become colorless. The product (210 mg, 47%) was isolated as a red solid. Anal. Calcd for $C_{92}H_{52}BClF_{26}Fe_2N_8O_2$ (**1**·BArF·C_5H_{12}): C, 56.57; H, 2.68; N: 5.74. Found: C, 56.29; H, 2.46; N, 5.80. ^{1}H NMR ($CDCl_3$, 300 MHz): δ 27−24 (br, methylene −CH_2−, PY-6H), 16.1 (br, pyrrole-H), 15.2−10 (PY-3H, PY-5H), 7.9−7.2 (*m*- and *p*-phenyl-H), 6.9−5.8 (PY-4H). UV−vis (CH_2Cl_2; λ_{max}, nm; ϵ, mol^{-1} L^{-1}): 328, 34000; 416, 105000; 569, 9300. FTIR (film, cm^{-1}): 2926, 2856, 1644, 1625, 1610, 1583, 1513, 1463, 1374, 1332, 1274, 1235, 1204, 1162, 1085, 1055, 1001, 984, 912, 887, 837, 798. MALDI-TOF-MS: *m*/*z* 1202 (M + H$^+$ − BArF$^-$)$^+$, *m*/*z* 1167 (M + H$^+$ − Cl$^-$ − BArF$^-$)$^+$.

[(^{6}L)Fe−O−Fe(Cl)]PF_6 (1·PF_6). A procedure identical to the one employed for the synthesis of **1**·BArF was utilized with the exception that $NaPF_6$ was used for metathesis. The product, obtained via a workup identical to that for **1**·BArF, resulted in the isolation of a red solid (150 mg, 49%). Anal. Calcd for $C_{63}H_{40}ClF_{12}Fe_2N_8O_2P$ (**1**·PF_6): C, 56.17; H, 2.99; N, 8.32. Found: C, 55.98; H, 2.97; N, 8.04. ^{1}H NMR ($CDCl_3$, 300 MHz): δ 28−24 (br, methylene −CH_2−, PY-6H), 17−14 (br, pyrrole-H), 12−11 (PY-3H, PY-5H), 9−8 (*m*- and *p*-phenyl-H), 6 (PY-4H). UV−vis (CH_2Cl_2; λ_{max}, nm): 326, 416, 568. MALDI-TOF-MS: *m*/*z* 1202 (M + H$^+$ − PF_6^-)$^+$, *m*/*z* 1167 (M + H$^+$ − Cl$^-$ − PF_6^-)$^+$. Crystals, suitable for X-ray diffraction, were obtained by layering a concentrated tetrahyrdrofuran solution of **1** with a mixture of methanol, pentane, and heptane (1:5:5). While the bulk of the material described in the synthesis (given above) is the pure chloride-containing complex, these X-ray-quality crystals are a mixture of a methoxide analogue [(^{6}L)Fe−O−Fe(MeO)]PF_6 (69%) and [(^{6}L)Fe−O−Fe(Cl)]PF_6 (31%). See Results and Discussion for further information.

[(^{5}L)Fe−O−Fe(Cl)]ClO_4 (2·ClO_4).[19] In a 50 mL airless flask, 201 mg (0.193 mmol) of ^{5}L (synthesized according to a published procedure)[17] was dissolved in 15 mL of degassed DMF and taken to reflux under an argon atmosphere. When the boiling point was reached, 170 mg (1.34 mmol, 3.5 equiv) of $FeCl_2$ was added as a solid. The reaction mixture was refluxed for an additional hour, after which time it had turned to an intense blood-red color. Subsequently, it was cooled to room temperature while being exposed to air. When cooled, 15 mL of a saturated NaCl solution was added, resulting in an immediate formation of a brown-red precipitate. The mixture was placed in the freezer (−20 °C) for 1 h. The precipitate was filtered over a compacted Celite plug on a glass frit and washed with distilled water until the washings were colorless. The frit with the precipitated material was then dried in vacuo, the solids were collected by rinsing them through the frit with CH_2Cl_2, and the solvent was removed on a rotary evaporator. The red solid was redissolved in 20 mL of CH_3CN. To this solution was added 50 mg of $NaClO_4$, dissolved in 2.5 mL of CH_3CN. The mixture was stirred for 30 min, then filtered over a Celite plug on a glass frit, and evaporated to dryness on the rotary evaporator. ^{1}H NMR and TLC indicated nearly pure Fe−O−Fe′, contaminated with a small amount of a paramagnetic product. The two products were separated on an alumina column (1.5 cm × 15 cm) using a methanol in dichloromethane gradient (2−3%). This procedure yielded 166.5 mg (66%) of **2** as a red-brown solid. This solid was recrystallized from CH_2Cl_2/heptane. Anal. Calcd for $C_{63}H_{41}N_8O_6F_6Cl_2Fe_2$·0.25$C_7H_{16}$: C, 58.62; H, 3.34; N, 8.45. Found: C, 58.51; H, 3.57; N, 8.07. ^{1}H NMR ($CDCl_3$, 300 MHz): δ 22−20 (br, methylene −CH_2−, PY-6H), 15.79 (br, pyrrole-H), 15.21, 12.4 (PY-3H, PY-5H), 7.6 (*m*- and *p*-phenyl-H), 6.50, 6.01, 5.73 (PY-4H). UV−vis (CH_2Cl_2; λ_{max}, nm; ϵ, mol^{-1} L^{-1}): 321, 38000; 413, 108000; 564, 10500. FTIR (KBr, cm^{-1}): 2926, 1622, 1607, 1584, 1464, 1333, 1273, 1235, 1103, 997, 837, 799, 716, 623, 579, 509. ESI-MS (CH_3CN solution): *m*/*z* 1201 (M − ClO_4^-)$^+$.

[(^{5}L-d_2)Fe−O−Fe(Cl)]ClO_4 (2-d_2·ClO_4). This complex was synthesized according to a literature procedure.[17] ^{2}H NMR ($CHCl_3$, 61 MHz): δ 5.84 (br, −CD_2O−).

[(^{5}L-d_{10})Fe−O−Fe(Cl)]ClO_4 (2-d_{10}·ClO_4). The synthesis of this compound was performed as described for **1**, except that ^{5}L-d_{10} was substituted for ^{5}L. The spectral data are as for **2**. ^{2}H NMR ($CHCl_3$, 61 MHz): δ 15.9 (pyrrole-D), 5.84 (br, −CD_2O−).

[(F_8)Fe−O−Fe(Cl)(TMPA)]ClO_4 (3·ClO_4).[19] In a 200 mL airless flask equipped with a stirring bar were mixed 98.7 mg (0.12 mmol) of (F_8)FeOH and 1 equiv (61 mg) of [(TMPA)$FeCl_2$]ClO_4 in 50 mL of acetone. The solids were stirred for 20 min under argon, and then 1 equiv (16 μL) of triethylamine, dissolved in 50 mL of degassed acetone, was introduced. The deep red, homogeneous reaction mixture was stirred under argon for 1 h, and then the acetone was removed under reduced pressure. The solid residue was redissolved in 30 mL of degassed CH_2Cl_2, filtered to remove precipitated Et_3N·HCl, and finally layered with 60 mL of degassed heptane. The complex crystallized as black needles (90 mg, 57%). Anal. Calcd for $C_{62}H_{38}N_8O_5F_8Cl_2Fe_2$: C, 56.86; H, 2.92; N, 8.56. Found: C, 56.44; H, 2.98; N, 8.48. ^{1}H NMR ($CDCl_3$, 300 MHz): δ 22−17.5 (br, PY-6H, methylene −CH_2−), 15.2 (pyrrole-H), 13.76, 13.16, 11.8, 10.9 (PY-3, PY-5), 7.75, 7.61, 7.40 (*m*- and *p*-phenyl-H), 6.1 (PY-4H). UV−vis (CH_2Cl_2; λ_{max}, nm; ϵ, mol^{-1} L^{-1}): 324, 34600; 411, 103700; 564, 10250. FTIR (KBr, cm^{-1}): 2926, 1624, 1607, 1574, 1464, 1445, 1331, 1273, 1235, 1098, 999, 837, 789, 714, 623, 579, 509. FAB-MS (*m*-nitrobenzyl alcohol matrix): *m*/*z* 1209 (M − ClO_4^-)$^+$. ESI-MS (CH_3CN solution): *m*/*z* 1209 (M − ClO_4^-)$^+$.

[(F_8)Fe−O−Fe(Cl)(TMPA-6,6′-d_2)]ClO_4 (4·ClO_4). A procedure identical to that described for the synthesis of **3** was followed, using [(TMPA-6,6′-d_2)$FeCl_2$]ClO_4 instead of [(TMPA)$FeCl_2$]ClO_4. Anal. Calcd for $C_{62}H_{36}D_2N_8O_5F_8Cl_2Fe_2$·0.5$CH_2Cl_2$·0.5$C_7H_{16}$: C, 56.45; H, 3.52; N, 7.98. Found: C, 55.99; H, 2.94; N, 7.93. The spectral data are similar to those for **3**. ^{2}H NMR ($CHCl_3$, 61 MHz): δ 19.58, 17.69.

[(F_8)Fe−O−Fe(Cl)(TMPA-d_6)]ClO_4 (5·ClO_4). A procedure identical to that described for the synthesis of **3** was followed, using [([(TMPA-d_6)$FeCl_2$]ClO_4 instead of [(TMPA)$FeCl_2$]ClO_4. Anal. Calcd for $C_{62}H_{32}D_6N_8O_5F_8Cl_2Fe_2$·$CH_2Cl_2$·$H_2O$: C, 53.34; H, 2.98; N, 7.90. Found: C, 53.29; H, 2.73; N, 7.68. The spectral data are as for **3**. ^{2}H NMR ($CHCl_3$, 61 MHz): δ 19.31, 11.56, 4.27. FAB-MS (*m*-nitrobenzyl alcohol matrix): *m*/*z* 1215 (M − ClO_4^-)$^+$.

[(F_8)Fe−O−Fe(Cl)(3-Me_3TMPA)]ClO_4 (6·ClO_4). A procedure identical to that described for the synthesis of **3** was followed, using [(3-Me_3TMPA)$FeCl_2$]ClO_4 instead of [(TMPA)$FeCl_2$]ClO_4. In the final crystallization step it was necessary to cool the CH_2Cl_2 mixture to −20 °C to obtain crystalline material. Anal. Calcd for $C_{65}H_{44}N_8O_5F_8Cl_2Fe_2$: C, 57.76; H, 3.28; 8.29. Found: C, 57.76, H, 3.39; N, 8.57. ^{1}H NMR ($CDCl_3$, 300 MHz): δ 22.5−17.5 (br,

Table 1. Summary of X-ray Crystallographic Data for **1**·PF_6

empirical formula	$C_{70}H_{57}ClF_{12}Fe_2N_8O_3P$	*V*, Å^3	2977.3(11)
fw	1464.36	Z	2
cryst size, mm	0.35 × 0.15 × 0.03	ρ_{calcd}, g cm^{-3}	1.633
cryst syst	triclinic	abs coeff, mm^{-1}	0.66
space group	$P\bar{1}$	max/min transm	1.00/0.84
T, K	150(2)	θ range, deg	1.25−28.31
a, Å	13.185(3)	no. of data	13078 [R_{int} = 0.0381]
b, Å	14.590(3)	no. of params	806
c, Å	16.885(4)	R1(*F*)[a] (*I* > 2σ(*I*))	0.1007
α, deg	104.219(4)	wR2(F^2)[b] (*I* > 2σ(*I*))	0.2337
β, deg	91.572(4)		
γ, deg	107.907(4)		

[a] $R1(F) = \sum||F_o| - |F_c||/\sum|F_o|$. [b] $wR2(F^2) = \{\sum[w(F_o^2 - F_c^2)^2]/\sum[w(F_o^2)^2]\}^{1/2}$; $w = 1/[\sigma^2(F_o^2) + (aP)^2 + bP]$; $P = [2F_c^2 + \max(F_o,0)]/3$.

PY-6H, methylene −CH_2−), 15.26 (pyrrole-H), 13.94, 13.65, 12.60 (PY-5H), 7.76, 7.63, 7.42 (*m*- and *p*-phenyl-H), 5.78 (PY-4H), 2.23 (−CH_3). FAB-MS (*m*-nitrobenzyl alcohol matrix): *m*/*z* 1251 (M − ClO_4^-)$^+$.

[(F_8-*d*$_8$)Fe−O−Fe(Cl)(3-Me_3TMPA)]ClO_4 (6-*d*$_8$·ClO_4). This compound was prepared as described for **3**, using (F_8-*d*$_8$)FeOH instead of (F_8)FeOH and [(3-Me_3TMPA)$FeCl_2$]ClO_4 instead of [(TMPA)$FeCl_2$]ClO_4. In the final crystallization step it was necessary to cool the CH_2Cl_2 mixture to −20 °C to obtain crystalline material. ^{1}H NMR ($CDCl_3$, 300 MHz): δ 22−17.5 (br, PY-6H, methylene −CH_2−), 15.19, 13.85, 13.66, 12.5, 11.5 (PY-5H), 7.73, 7.62, 7.42 (*m*- and *p*-phenyl-H), 5.76 (PY-4H), 2.22 (−CH_3). ^{2}H NMR ($CHCl_3$, 61 MHz): δ 15.28 (pyrrole-D). FTIR (KBr, cm^{-1}): 3081, 2924, 2855, 1622, 1588, 1464, 1331, 1275, 1236, 1101, 999, 930, 847, 787, 764, 716, 623, 575, 509.

[(F_8-*d*$_8$)Fe−O−Fe(Cl)(4-Me_3TMPA)]ClO_4 (7-*d*$_8$·ClO_4). This compound was prepared as described for **3**, using (F_8-*d*$_8$)FeOH instead of (F_8)FeOH and [(4-Me_3TMPA)$FeCl_2$]ClO_4 instead of [(TMPA)$FeCl_2$]ClO_4. In the final crystallization step it was necessary to cool the CH_2Cl_2 mixture to −20 °C to obtain crystalline material. Anal. Calcd for $C_{65}H_{36}D_8N_8O_5F_8Cl_2Fe_2$·$H_2O$: C, 56.66; H, 3.39; 8.13. Found: C, 56.22, H, 3.15; N, 8.05. ^{1}H NMR ($CDCl_3$, 300 MHz): δ 22−17.5 (br, PY-6H, methylene −CH_2−), 15.16, 14.83, 14.4, 13.42, 12.76, 11.60 (PY-3H, PY-5H), 7.76, 7.62, 7.43 (*m*- and *p*-phenyl-H), 2.8, 2.49 (−CH_3). ^{2}H NMR ($CHCl_3$, 61 MHz): δ 15.17 (pyrrole-D). FTIR (KBr, cm^{-1}): 2924, 1620, 1584, 1464, 1329, 1275, 1236, 1099, 999, 849, 787, 766, 716, 623, 575, 509.

[(F_8-*d*$_8$)Fe−O−Fe(Cl)(5-Me_3TMPA)]ClO_4 (8-*d*$_8$·ClO_4). This compound was prepared as described for **3** using (F_8-*d*$_8$)FeOH instead of (F_8)FeOH and [(5-Me_3TMPA)$FeCl_2$]ClO_4 instead of [(TMPA)$FeCl_2$]ClO_4. In the final crystallization step it was necessary to cool the mixture to −20 °C to obtain crystalline material. Anal. Calcd for $C_{65}H_{36}D_8N_8O_5F_8Cl_2Fe_2$·$H_2O$: C, 56.66; H, 3.39; 8.13. Found: C, 56.90, H, 3.44; N, 7.96. ^{1}H NMR ($CDCl_3$, 300 MHz): δ 22−17.5 (br, PY-6H, methylene −CH_2−), 15.38, 14.63, 13.76, 11.10 (PY-3H), 7.77, 7.62, 7.44 (*m*- and *p*-phenyl-H), 6.69, 6.48, 6.08, 5.79 (PY-4H), 2.63, 2.40, 2.15 (−CH_3). ^{2}H NMR ($CHCl_3$, 61 MHz): δ 15.38 (pyrrole-D). FTIR (KBr, cm^{-1}): 2924, 1624, 1580, 1497, 1464, 1327, 1275, 1235, 1103, 999, 837, 787, 764, 716, 662, 623, 575, 509.

X-ray Crystallography. The complex **1**·PF_6 was crystallized by liquid diffusion of a methanol/pentane/heptane mixture into a concentrated tetrahydrofuran solution. A suitable crystal of **1**·PF_6 was mounted with epoxy cement to the tip of a glass fiber. Intensity data were collected at 150(2) K with a Bruker SMART APEX CCD diffractometer with graphite-monochromated Mo Kα radiation (λ = 0.71073 Å).

An absorption correction was done using the SADABS program (Sheldrick, G. M. SADABS (2.01), Bruker/Siemens Area Detector Absorption Correction Program, Bruker AXS, Madison, WI, 1998). The structure was solved by direct methods, completed by difference Fourier syntheses, and refined by full-matrix least-squares refinement procedures based on F^2. All non-hydrogen atoms were refined with anisotropic thermal parameters. The hydrogen atoms were assigned idealized geometric positions and refined in a rigid group model. Two highly disordered heptane and/or pentane solvent molecules were treated by the SQUEEZE program (Van der Sluis, P.; Spek, A. L. *Acta Crystallogr., Sect. A* **1990**, *A46*, 194−201). Correction of the X-ray data by SQUEEZE (96 electrons/cell) was close to the required value (100 electrons/cell for heptane/pentane occupation). One coordination site at the non-heme iron Fe(2) atom is occupied by either a Cl atom or an O atom (of a −OMe group) in a ratio of 31:69. All software and sources of the scattering factors are contained in the SHELXTL (5.1) program library (G. Sheldrick, Siemens XRD, Madison, WI). Relevant crystallographic information and the main details of the diffraction experiment and refinement of the crystal structure are provided in Table 1, while the full X-ray structural report, in CIF format, may be found in the Supporting Information.

Resonance Raman (RR) Spectroscopy. RR samples were prepared by dissolving samples of **1**·BArF in either 20% $H_2{}^{16}O$/CH_3CN or 20% $H_2{}^{18}O$/CH_3CN. RR spectra were obtained at room temperature using 442 nm excitation from a He−Cd laser (Liconix 4240NB, Santa Clara, CA). The backscattered light was analyzed with a McPherson (Acton, MA) 2061/207 spectrograph (0.67 m with variable gratings) equipped with a Princeton Instrument (Roper Scientific, Trenton, NJ) liquid-nitrogen-cooled (LN-1100PB) charge-coupled device (CCD) detector. Frequencies were calibrated relative to known standards and are within ±1 cm^{-1}. The laser power was kept below 20 mW to minimize sample decomposition and to prevent undesirable photochemical side reactions.

Mössbauer Spectroscopy. ^{57}Fe Mössbauer spectra were measured with an Oxford Instruments Mössbauer spectrometer in constant motion mode, using ^{57}Co/Rh as the radiation source. The minimum experimental line widths were 0.24 mm/s. The temperature of the samples was controlled by an Oxford Instruments Variox Cryostat. Isomer shifts were determined relative to that of α-iron at 300 K. The measurements were carried out at 80 K with solid samples containing natural-abundance ^{57}Fe.

Magnetic Susceptibility Measurements. Magnetic susceptibility data for polycrystalline samples of selected Fe−O−Fe′ systems were collected in the temperature range 2−295 K to characterize the sign and magnitude of the magnetic exchange interaction at 1, 2, 4, or 7 T on a Quantum Design SQUID-Magnetometer MPMS. The samples were isolated in gelatin capsules, and the response function was measured four times for each given temperature, yielding a total of 32 measured points. The resulting volume magnetization from the samples had its diamagnetic contribution compensated and was recalculated as volume susceptibility. Dia-

magnetic contributions were estimated for each compound by making use of Pascal's constants.

The analysis of the magnetic data was performed using the Heisenberg−Dirac−van Vleck (HDvV) model. A least-squares fitting computer program[45] with a full-matrix diagonalization approach was employed to fit the temperature-dependent magnetization. The software uses the spin Hamiltonian operator $\mathbf{H}_{total} = \mathbf{H}_Z + \mathbf{H}_{ZFS} + \mathbf{H}_{HDvV}$, where the exchange coupling is described by $\mathbf{H}_{HDvV} = -2JS_1 \cdot S_2$, the Zeeman interactions are given by $\mathbf{H}_Z = \mu_B B g_i S_i$, and the axial single-ion zero-field interaction is described by $\mathbf{H}_{ZFS} = DS_Z^2$. The latter term is included only when necessary. The coupling constant J describes the energy gap between the ground term and the first excited state and results from both antiferromagnetic and ferromagnetic exchange interactions, with $J = J_{AF} + J_F$.

Results and Discussion

Synthesis. The procedures for synthesizing the free-base porphyrins $(F_8)H_2$[41,46] and $(F_8\text{-}d_8)H_2$[41] as well as the free-base ligands ^{5}L[17] and ^{6}L[17] have been previously reported. TMPA and its various methylated or deuterated derivatives were prepared as reported in the literature, and the iron(III) complexes were synthesized following procedures similar to those described by Que and co-workers.[47,48] The "untethered" Fe−O−Fe′ complexes were formed via acid−base self-assembly chemistry (Scheme 1), by mixing equimolar amounts of the ferric hydroxide porphyrin with ferric TMPA in the presence of a base. The tethered, constitutionally isomeric ligands ^{5}L and ^{6}L were employed to examine what effects the steric constraints of an ether linkage would have on the structural, spectroscopic, and magnetic properties of these mixed-moiety Fe−O−Fe′ complexes [(^{6}L)Fe−O−Fe(Cl)]$^+$ (**1**) and [(^{5}L)Fe−O−Fe(Cl)]$^+$ (**2**) (Scheme 1). Direct metalation with iron of the ligand ^{5}L, followed by column chromatography and metathesis, affords either **2**·ClO_4 or by analogy the deuterated ^{5}L derivative **2**-d_2·ClO_4 or **2**-d_{10}·ClO_4. The synthesis of **1**·BArF and **1**·PF_6 requires a slightly modified procedure relative to that of **2**, as complex **1** does not survive purification by column chromatography. Addition of 1 equiv of ferrous chloride and 1 equiv of MX (where M = Na^+ or Li^+ and X = $B(C_6F_5)_4^-$ or PF_6^-) to the reduced empty tether porphyrin complex (^{6}L)Fe^{II} [16] in THF, followed by exposure to the ambient atmosphere, allows for the clean isolation of **1** after repeated recrystallization.

Absorption Spectroscopy. The optical absorption spectra of **1** and **2** are virtually identical, with very intense Soret (B) transitions at $\lambda_{max} = 416$ ($\epsilon = 105000$ M^{-1} cm^{-1}) and 413 ($\epsilon = 108000$ M^{-1} cm^{-1}) nm for **1** and **2**, respectively. Of lesser intensity are the α-bands (Q-bands), found at $\lambda_{max} = 569$ ($\epsilon = 9300$ M^{-1} cm^{-1}) and 564 ($\epsilon = 10500$ M^{-1} cm^{-1}) nm for **1** and **2**, respectively. Both of these series of bands arise from porphyrin-based $\pi \rightarrow \pi^*$ transitions, according to Gouterman's four-orbital model,[49] and are similar to those observed for other ferric porphyrin complexes. It should be noted that a band near $\lambda_{max} = 413$ or 416 nm differs from a typical heme−oxo (O^{2-}) dimer (e.g., $[(F_8)Fe]_2O$) Soret which is found at $\lambda_{max} = 400$ nm,[41] providing support that both **1** and **2** remain intramolecular heme/non-heme Fe−O−Fe′ species in solution. Finally, ligand-to-metal charge-transfer (LMCT; O → Fe) bands are found in the oxo (O^{2-}) dimer region at $\lambda_{max} = 328$ ($\epsilon = 34000$ M^{-1} cm^{-1}) and 321 ($\epsilon = 38000$ M^{-1} cm^{-1}) nm for **1** and **2**, respectively, and are of typical intensity ($\epsilon \approx 7000-10000$ M^{-1} cm^{-1}) for LMCT bands of this nature.[21] We observe only the signals from the heme iron; typical non-heme iron complexes of the general formula [(TMPA)Fe(Cl)]$_2O^{2+}$ exhibit rather weak chloride-to-iron charge-transfer bands near 380 nm ($\epsilon \approx 3000$ M^{-1} cm^{-1}).[47] Such electronic transitions are overlapped by the highly intense Soret transitions.

Scheme 1

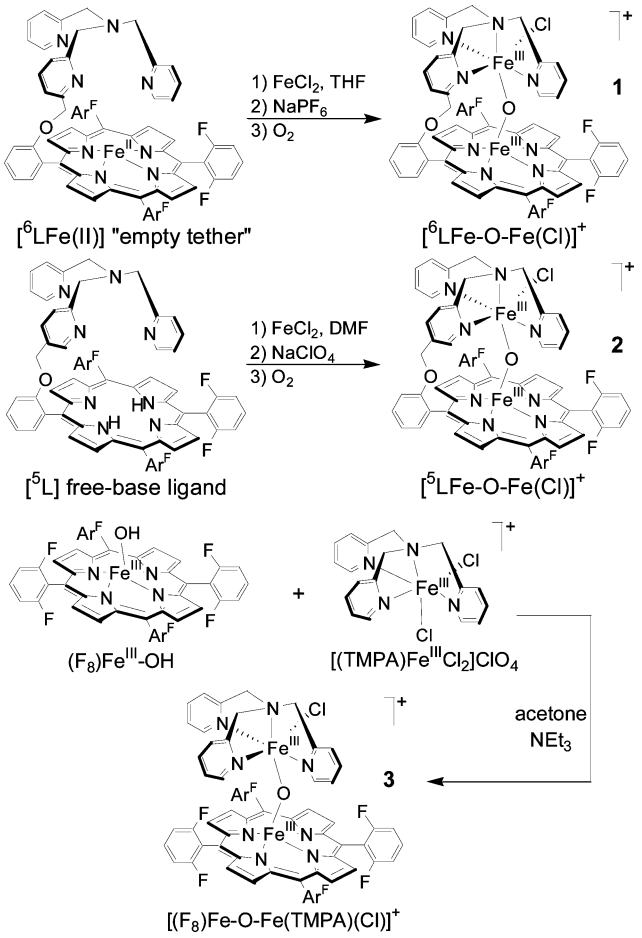

X-ray Crystallography. A crystal of **1**·PF_6 cocrystallized with [(^{6}L)Fe−O−Fe(CH_3O)]PF_6 in a 31:69 ratio and was amenable to an X-ray structural determination. Undoubtedly, the methoxy-ligand-containing complex derives from the crystallization of **1**·PF_6 from methanol (in our attempt to obtain X-ray-quality crystals). Interestingly, the structure for **1**·PF_6, Figure 2, reveals a slightly bent ($\angle = 166.7(3)°$) Fe−O−Fe′ moiety spanning the heme/non-heme ^{6}L ligand (Table 2); both **2**·ClO_4 and the untethered **3**·ClO_4 have significantly bent ($\angle \approx 157°$) Fe−O−Fe′ moieties.[19] The nonlinearity of the monobridged Fe−O−Fe′ is a feature both

(45) Krebs, C. Ph.D. Thesis, Ruhr-Universität, Bochum, Germany, 1997.
(46) Nanthakumar, A.; Goff, H. M. *Inorg. Chem.* **1991**, *30*, 4460−4464.
(47) Kojima, T.; Leising, R. A.; Yan, S.; Que, L., Jr. *J. Am. Chem. Soc.* **1993**, *115*, 11328−11335.
(48) Chen, K.; Que, L., Jr. *J. Am. Chem. Soc.* **2001**, *123*, 6327−6337.
(49) Gouterman, M. *J. Mol. Spectrosc.* **1961**, *6*, 138−163.

Table 2. Selected Bond Distances (Å) and Bond Angles (deg) for **1**·PF_6, **2**·ClO_4, and **3**·ClO_4[a]

	1·PF_6	***2***·ClO_4[b]	***3***·ClO_4[b]
	(a) Bond Distances (Å)		
Fe(1)−O(1)	1.785(4)	1.771(14)	1.776(13)
Fe(2)−O(1)	1.795(5)	1.783(14)	1.765(13)
Fe(1)−N	2.067(5)−2.081(5)	2.079(17)−2.090(18)	2.069(22)−2.114(22)
Fe(2)−N	2.187(6)−2.277(5)	2.128(18)−2.263(19)	2.159(22)−2.254(22)
Fe(1)···Fe(2)	3.556(1)	3.484(6)	3.468(5)
	(b) Bond Angles (deg)		
Fe(1)−O(1)−Fe(2)	166.7(3)	157.3(9)	156.8(9)
Cl(1)−Fe(2)−N(7)	167.2(2)	164.9(5)	170.4(7)
O(1)−Fe(2)−N(6)	166.9(2)	165.0(7)	165.1(7)

[a] The atom numbering scheme corresponds to the ORTEP diagram for **1**, Figure 2. [b] Reference 19.

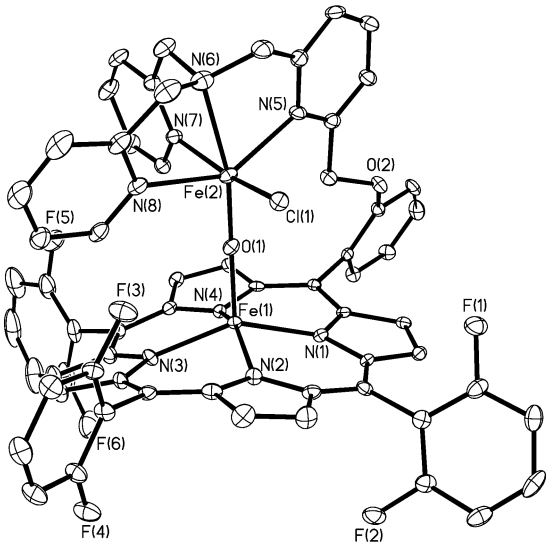

Figure 2. ORTEP view of the cation **1** showing 30% probability thermal ellipsoids. The hydrogen atoms are omitted for clarity.

unexpected and unique to these heme/non-heme diiron complexes; both heme−oxo−heme and (TMPA)Fe−oxo−Fe(TMPA) compounds have linear Fe−O−Fe′ structures (see entries in Table 4). The Fe−O−Fe′ unit in the structure of **1** (relative to **2**·ClO_4 or **3**·ClO_4) results in an Fe···Fe′ separation of 3.556(1) Å, while **2** and **3** have slightly shorter Fe···Fe′ distances (av ∼3.47 Å).[19] The ferric heme iron in **1** is ligated by four pyrrole nitrogens in a distorted square-planar geometry, with the iron lying 0.54 Å out of the plane of the porphyrin macrocycle, consistent with that observed for other high-spin iron(III) porphyrinates.[50] Other structural parameters include ∠(N−Fe−N)(av) = 86.1(2)° and *d*(Fe−N_4)(av) = 2.074(7) Å. The fifth, apical (and bridging) oxo (O^{2-}) ligand has *d*(Fe−O) = 1.785(4) Å. The Fe−N distances are comparable to those of Fe−O−Fe′-bridged symmetric ferric heme species ([(TPP)Fe]$_2$O, *d*(Fe−N)(av) = 2.087 Å; [(F_8)Fe]$_2$O, *d*(Fe−N)(av) = 2.082 Å).[41] For all heme/non-heme diiron complexes, the heme Fe(1)−O bond distance is slightly shorter than the non-heme Fe(2)−O bond length (see Table 2 for a comparative summary).

The non-heme iron in **1**·PF_6 is hexacoordinated, with a distorted octahedral geometry. It is coordinated by three pyridyl nitrogens [*d*(Fe(2)−N)(av) = 2.22(5) Å], the alkylamine nitrogen [*d*(Fe(2)−N(6)) = 2.267(6) Å], and the bridging oxo (O^{2-}) ligand [*d*(Fe(2)−O(1)) = 1.795(5) Å, ∠(Fe(1)−O(1)−Fe(2)) = 166.7(3)°]. The amine nitrogen ligand, located *trans* to the oxo bridge, has the longest Fe−N distance (2.267(6) Å), similar to that observed for the Fe−N_{amine} bond in [(TMPA)Fe(Cl)]$_2O^+$ (2.263(6) Å). It is interesting to note the asymmetry imposed by the tethered pyridyl ring; the Fe(2)−N(5) bond, the non-heme iron bonded to the tethered pyridyl arm, has a long distance of 2.227(5) Å. When compared to the much shorter Fe(2)−N(8) distance of 2.187(6) Å for the untethered pyridyl arm (located *trans* to the tethered arm), it is evident that, by placing a substituent in the 6-pyridyl position on one of the rings, steric effects limit the pyridine nitrogen from approaching the iron center, undoubtedly influencing the overall geometry of the Fe−O−Fe′ moiety. A similar geometric change and Fe−$N_{pyridyl}$ bond elongation, forced by a substituent in the 6-pyridyl position, are also noted when the isomeric heme−Cu complexes [(^{5}L)Fe−O−Cu]ClO_4 and [(^{6}L)Fe−O−Cu]ClO_4, where the Fe−O−Cu angle is 141 ± 6° or 171.1(3)°, respectively, are compared.[16,17] The (elongated) pyridyl and amine Fe−N bond distances found in **1**·PF_6 are typical for ferric 6-Me$_n$TMPA complexes,[37] while the Fe−Cl distance is also comparable to literature values for similar compounds.[32,47,51] The Fe(2)−O(1) distance, 1.795(5) Å, is similar to the Fe−O distance (1.790 Å) in the previously reported *μ*-oxo [(TMPA)$_2$Fe$_2$(Cl)$_2$O]$^{2+}$ dinuclear complex.[47]

As mentioned, the X-ray crystal structure for **1**·PF_6 reveals that a chloride ion is coordinated to the non-heme iron with 31% site occupation. The remaining 69% of this site is occupied by a methoxide ligand, derived from the crystallization solvent. However, the inclusion of either a chloride or methoxide ligand [*d*(Fe(2)−O(3)) = 1.918(8) Å] at the non-heme iron does not alter the ∠(Fe−O−Fe′) unit, nor are other structural parameters changed. An ORTEP representation of the complex [(^{6}L)Fe−O−Fe(OMe)]PF_6 is found in the Supporting Information. Further efforts are under way to isolate the pure complex [(^{6}L)Fe−O−Fe(OMe)]PF_6.

Resonance Raman Spectroscopy. The Fe−O−Fe′ moiety, when considered an independent vibrational entity, has three possible vibrational modes: (i) an asymmetric Fe−O−Fe′ stretch (ν_{as}), (ii) a symmetric Fe−O−Fe′ stretch (ν_s), and (iii) an Fe−O−Fe′ bend.[21] Oxo-bridged (O^{2-})

(50) Scheidt, W. R. R., C. A. *Chem. Rev.* **1981**, *81*, 543−555.

(51) Yan, S.; Cox, D. D.; Pearce, L. L.; Juarez-Garcia, C.; Que, L., Jr.; Zhang, J. H.; O'Connor, C. J. *Inorg. Chem.* **1989**, *28*, 2509−2511.

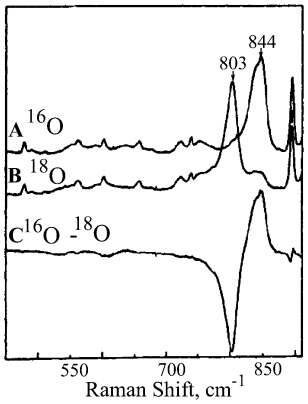

Figure 3. Low-frequency resonance Raman spectra of **1**·BArF, prepared in 20% $H_2{}^{16}O$/acetonitrile (trace A) or 20% $H_2{}^{18}O$/acetonitrile (trace B).

diferric compounds adopting a bent geometry exhibit a symmetric stretch, ν_s(Fe−O−Fe′), at ∼400 cm^{-1} and an asymmetric stretch, ν_{as}(Fe−O−Fe′), at ∼850 cm^{-1} that are both IR- and Raman-active.[52,53] Studies on non-heme oxo-bridged diiron(III) complexes have revealed that nonequivalent ligand sets give RR spectra with a large I_{as}/I_s ratio (I_{as}/I_s = the signal intensity ratio between asymmetric and symmetric stretches).[54,55]

Soret (B) excitation of an acetonitrile/water solution of **1**·BArF at 442 nm results in a typical porphyrin RR spectrum dominated by strong high-frequency porphyrin skeletal modes, characteristic of a pentacoordinate high-spin ferric species, along with weaker iron−ligand vibrations.[18,53,56] The low-frequency RR spectra of **1**·BArF are shown in Figure 3, with spectrum A resulting from the addition of 20% $H_2{}^{16}O$ and spectrum B resulting from the addition of 20% $H_2{}^{18}O$; spectrum C represents the difference (spectrum A − spectrum B). The data thus reveal an asymmetric stretch ν_{as}(Fe−O−Fe′) at 844 cm^{-1}, which is down-shifted 41 cm^{-1} upon the formation of an Fe−^{18}O−Fe′ bridge. As has previously been observed in both the enzyme NOR and **2**·BArF,[14] the asymmetric vibration is strongly resonance enhanced, while the symmetric vibration sees no resonance enhancements and is not observed. The slightly bent nature of the Fe−O−Fe′ bridge in **1** and **2** yields ν_{as} values that are consistent with the observed Fe−O−Fe′ angles in these complexes.[54] For comparison, data for several other complexes with Fe−O−Fe′ bridges are presented in Table 3, revealing that the parameters for complexes **1** and **2** compare and correlate well with those for μ-oxo (O^{2-}) porphyrin and non-heme iron synthetic complexes. The presence of a heme/non-heme Fe−O−Fe′ RR signature in **1**·BArF, similar to the heme/non-heme Fe−O−Fe′ RR signal from the NOR enzyme, suggests that **1**·BArF represents a good oxidized active site model for the resting state in NOR.[14]

Table 3. Resonance Raman and Fe−O−Fe′ Angle (deg) Data for NOR, Synthetic Complexes **1**·BArF and **2**·BArF, and Several Related Complexes

complex	ν_{as}(Fe−O−Fe′)-(^{16}O)(Δ(^{18}O)) (cm^{-1})	∠(Fe−O−Fe′) (deg)	ref
NOR	810(30)	145[a]	14
[(^{6}L)Fe−O−Fe(Cl)]$^+$ (**1**)	844(41)	166.7	this work
[(^{5}L)Fe−O−Fe(Cl)]$^+$ (**2**)	841(40)	157.3	14
[(TPP)Fe]$_2$O	885	175	57
[(SALEN)Fe]$_2$O	832	144.6	21
{[(TMPA)Fe]$_2$O(OAc)}$^{3+}$	770	129	51
{[(TACN)Fe]$_2$O(OAc)$_2$}$^{2+}$	749	118.7	21

[a] Estimated from ν_{as}(Fe−O−Fe′).

Mössbauer Spectroscopy. The Mössbauer spectra of complexes **1**·BArF, **3**·ClO_4, and **6**·ClO_4 are shown in Figure 4 at 80 K and are comparable to that recorded for **3**·ClO_4 at room temperature, which was previously reported by this group.[19] Each of these spectra reveals a pair of doublets characteristic of bimetallic species containing high-spin iron(III) centers in different environments. A summary of Mössbauer parameters is given in Table 4. Site A presents isomer shifts (δ) ranging from 0.39 to 0.40 mm/s and quadrupole splittings (ΔE) ranging from 0.45 to 0.64 mm/s and is attributed to a "heme-type" environment. Site B presents small variations in δ values from 0.44 to 0.45 mm/s with ΔE values from 1.45 to 1.67 mm/s and is attributed to a less symmetric, "non-heme-type" environment. The assignments are based upon previous values reported in the literature in which high-spin ferric-heme-type sites are near δ = 0.41 and ΔE = 0.67 mm/s,[21,58] whereas similar non-heme-type sites are found near δ = 0.45−0.50 mm/s and ΔE= 1.4−1.7 mm/s.[32,59] As a comparative example, intermediate-spin heme-type sites with S = 3/2 were reported recently showing δ values as high as 3.02 mm/s.[60]

At room temperature complexes **1**·BArF and **3**·ClO_4 show spectra with a 1:1 ratio between the two high-spin iron(III) sites. Interestingly, at 80 K, complexes **3**·ClO_4 and **6**·ClO_4 exhibit a ca. 30−50% excess of the heme-type site. Since clean elemental analyses and magnetization studies were obtained, we investigated the behavior of **6**·ClO_4 at 4.2 K, where, as expected, a 1:1 ratio was found.

Magnetism. The magnetic behavior of microcrystalline compounds **1**·BArF, **3**·ClO_4, and **6**·ClO_4 was measured and is summarized in Table 4. Figure 5 provides data for the complex **3**·ClO_4; the figures with data for **1**·BArF and **6**·ClO_4 are found in the Supporting Information.

At 290 K, the compound **1**·BArF exhibits a $\chi_{mol}T$ value of 0.92 emu K mol^{-1}, which is considerably lower than the

(52) Spiro, T. G.; Li, Y.-Y. In *Resonance Raman Spectroscopy of Metalloporphyrins*; Spiro, T. G., Ed.; Wiley-Interscience: New York, 1988; Vol. 3, pp 1−38.
(53) Nakamoto, K. *Infrared and Raman Spectra of Inorganic and Coordination Compounds*; Wiley-Interscience: New York, 1997.
(54) Sanders-Loehr, J.; Wheeler, W. D.; Shiemke, A. K.; Averill, B. A.; Loehr, T. M. *J. Am. Chem. Soc.* **1989**, *111*, 8084−8093.
(55) Gomez-Romero, R.; Witten, E. H.; Reiff, W. M.; Backes, G.; Sanders-Loehr, J.; Jameson, G. B. *J. Am. Chem. Soc.* **1989**, *111*, 9039−9047.
(56) Ghiladi, R. A.; Hatwell, K. R.; Karlin, K. D.; Huang, H.-w.; Moënne-Loccoz, P.; Krebs, C.; Huynh, B. H.; Marzilli, L. A.; Cotter, R. J.; Kaderli, S.; Zuberbuehler, A. D. *J. Am. Chem. Soc.* **2001**, *123*, 6183−6184.
(57) Burke, J. M.; Kincaid, J. R.; Spiro, T. G. *J. Am. Chem. Soc.* **1978**, *100*, 6077−6083.
(58) Strauss, S. H.; Pawlik, M. J.; Skowyra, J.; Kennedy, J. R.; Anderson, O. P.; Spartalian, K.; Dye, J. L. *Inorg. Chem.* **1987**, *26*, 724−730.
(59) Yan, S.; Cox, D. D.; Pearce, L. L.; Juarez-Garcia, C.; Que, L., Jr.; Zhang, J. H.; O'Connor, C. J. *Inorg. Chem.* **1989**, *28*, 2507−2509.
(60) Ohgo, Y.; Neya, S.; Ikeue, T.; Takahashi, M.; Takeda, M.; Funasaki, N.; Nakamura, M. *Inorg. Chem.* **2002**, *41*, 4627−4629.

Table 4. Structural, Magnetic, and Mössbauer Data for **1**·BArF, **2**·ClO_4, **3**·ClO_4, **6**·ClO_4, and Selected Synthetic Diferric Compounds

	d(Fe−O) (Å)	d(Fe···Fe′) (Å)	∠(Fe−O−Fe′) (deg)	$-J$ (cm^{-1})	δ_{Fe} (mm/s)	ΔE_A (mm/s)	ref
$[(^6L)Fe-O-Fe(Cl)]^+$ (**1**)	1.785, 1.795	3.556	166.7	115	0.47, 0.41[a]	1.59, 0.55[a]	this work
$[(^5L)Fe-O-Fe(Cl)]^+$ (**2**)	1.771, 1.783	3.484	157.3		0.45, 0.41[b]	1.32, 0.68[b]	19
$[(F_8)Fe-O-Fe(Cl)(TMPA)]^+$ (**3**)	1.776, 1.765	3.468	156.8	108	0.45, 0.40[b]	1.45, 0.56[b]	19
$[(F_8)Fe-O-Fe(Cl)(3\text{-}Me_3TMPA)]^+$ (**6**)				112	0.441, 0.393[a]	1.486, 0.453[a]	this work
$[(F_8)Fe-O-Fe(Cl)(3\text{-}Me_3TMPA)]^+$ (**6**)					0.454, 0.396[c]	1.497, 0.493[c]	this work
$[(SALEN)Fe]_2O$	1.78	3.391	144.6	89−92			21
$[(\mu\text{-XDK})(\mu\text{-O})Fe_2(HFAC)_2(H_2O)_2]$	1.792, 1.796	3.1794	124.82		0.58	1.68	33
$\{[(TMPA)(Cl)Fe]_2O\}^{2+}$	1.790	3.581	179.98	116			47
$\{(H_2O)(ClO_4)[(TMPA)Fe]_2O\}^{3+}$	1.791, 1.783	3.570	174.1				36
$\{[(TMPA)Fe]_2O(OAc)\}^{3+}$	1.80, 1.790	3.243	129.2	114	0.45	1.45	51
$\{[(H_2O)_5Fe]_2O\}^{4+}$	1.775	3.549	170.2	107	0.52	1.69	61
$\{[(TACN)Fe]_2O(OAc)_2\}^{2+}$	1.78	3.064	118.3		0.46	1.72	21
$[(TPP)Fe]_2O$	1.759	3.516	176.1	136	0.41	0.67	21
$[(F_8)Fe]_2O$	1.760	3.518	178.5	146			41
$[(F_{20})Fe]_2O$				147			62

[a] Recorded at 80 K. [b] Recorded at room temperature. [c] Recorded at 4.2 K. See the text for further explanation.

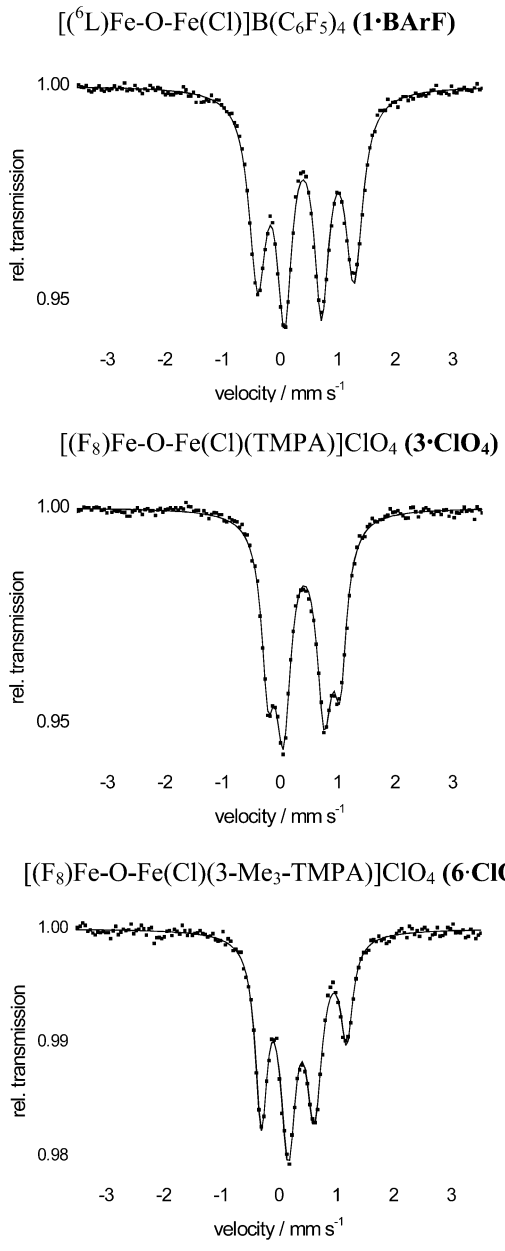

Figure 4. Mössbauer spectra of **1**·BArF, **3**·ClO_4, and **6**·ClO_4. The solid line is a least-squares fit of the data in each case.

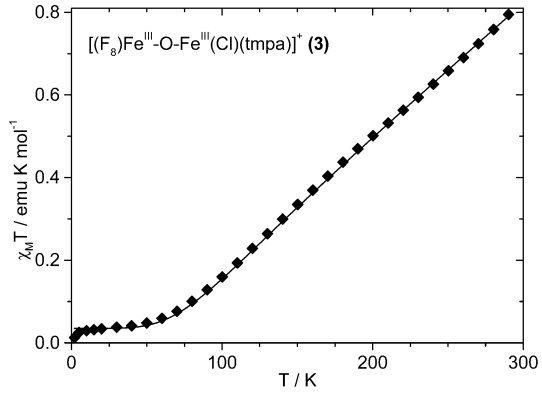

Figure 5. Magnetochemical behavior of the complex **3**·ClO_4. Similar results were obtained for **1**·BArF and **6**·ClO_4. The tilted squares denote the measured magnetization, while the solid line is the simulation of the data.

theoretical value of $\chi_{mol}T = 8.75$ emu K mol^{-1} expected for two noncoupled iron centers with $S_{Fe} = 5/2$. On lowering the temperature from 290 to 80 K, the values of $\chi_{mol}T$ decrease monotonically, approaching a plateau. This behavior indicates that the two iron centers in this complex are coupled antiferromagnetically. The residual magnetism observed at low temperature is attributed to paramagnetic impurities, possibly related to the presence of a small amount of parent $(^6L)Fe^{III}$ empty tether compound.[42] Indeed, despite several recrystallizations, and a consistent elemental analysis, the fitting of the magnetic properties of **1**·BArF required the inclusion of ca. 6% impurity. Nevertheless, the simulation of the experimental data serves the purpose of assessing the magnitude of exchange coupling between the iron centers present in the compound. The best fit yields $J = -114.82$ cm^{-1}, with $g_{Fe1} = g_{Fe2} = 2.0$, and confirms the antiferromagnetic nature of the couplings.

The complexes **3**·ClO_4 and **6**·ClO_4 exhibit similar behavior at 290 K with $\chi_{mol}T$ values of 0.79 and 0.74 emu K mol^{-1}, respectively. Similarly, the values are lower than the theoretical value expected for two noncoupled high-spin Fe(III) centers. Lowering the temperature to 50 K decreases the $\chi_{mol}T$ monotonically to 0.047 emu K mol^{-1} for **3**·ClO_4 and 0.025 emu K mol^{-1} for **6**·ClO_4. Over the range 50−5 K the curve stabilizes in a plateau near zero (Figure 5), as expected for an $S = 0$ ground state with antiferromagnetic

Table 5. ^{1}H NMR Data and Assignments for Compounds **1**·BArF, **2**·ClO_4, **3**·ClO_4, **6**-d_8·ClO_4, **7**-d_8·ClO_4, and **8**-d_8·ClO_4

assignment	**1**	**2**	**3**	**6**	**7**	**8**
TMPA-CH_2	27−24	22−20	22−17.5	22−17.5	22−17.5	22−17.5
pyrrole-H	16.1	15.79	15.2	a	a	a
PY-3H, PY-5H	15.2	15.21		15.19	15.16	15.38
PY-3H, PY-5H	14.9				14.83	14.63
PY-3H, PY-5H	14.5		13.76	13.85	14.4	13.76
PY-3H, PY-5H	13		13.16	13.66	13.42	
PY-3H, PY-5H	12	12.4	11.8	12.5	12.76	
PY-3H, PY-5H	10.5		10.9	11.5	11.60	11.10
m- and *p*-phenyl-H	7.9	7.6	7.75	7.73	7.76	7.77
m- and *p*-phenyl-H	7.5		7.61	7.62	7.62	7.62
m- and *p*-phenyl-H	7.2		7.40	7.42	7.43	7.44
PY-4H						6.69
PY-4H	6.9	6.50				6.48
PY-4H	6.7	6.01	6.10			6.08
PY-4H	5.79	5.73		5.76		5.79
TMPA-CH_3					2.8	2.63
TMPA-CH_3					2.49	2.40
TMPA-CH_3				2.22		2.15

[a] Resonance absent in the ^{1}H NMR spectrum due to the deuterium label.

coupling. Below 5 K the curve decreases drastically. The best fit values yield $J = -108$ cm^{-1} for **3** and $J = -112$ cm^{-1} for **6**·ClO_4 with $g_{Fe1} = g_{Fe2} = 2.0$ for both systems. Paramagnetic impurities ($S = 5/2$) of 0.8% and 0.3%, respectively, were included in these fits. The complexes **1**·BArF, **3**·ClO_4, and **6**·ClO_4 present Fe···Fe separations of ca. 3.50 Å, preventing any direct interaction between the two spin carriers.[63] Consequently, the observed spin coupling arises via superexchange along the Fe−O−Fe′ pathway.

Comparing the extent of magnetic coupling (i.e., $-J$ values) for **1**·BArF, **3**·ClO_4, and **6**·ClO_4 to the heme−oxo dimer and non-heme iron−oxo species (Table 4), the data reveal the heme/non-heme diiron complexes have weaker coupling than the strongly coupled heme−oxo−heme species ($-J = 136-147$ cm^{-1}). Typical non-heme iron−oxo−iron species have observed couplings $-J = 90-115$ cm^{-1}. Thus, our heme/non-heme diiron complexes exhibit electronic interactions more similar to those of non-heme iron−oxo species. The presence of electron-donating methyl groups attached to the pyridine rings of the ligand TMPA, as in the complex **6**·ClO_4, has little effect on the magnetic coupling compared to that of the unsubstituted complex **3**·ClO_4.

Nuclear Magnetic Resonance Studies. The ^{1}H NMR spectral data for compounds **1**·BArF, **2**·ClO_4, and **3**·ClO_4 are presented in Table 5. As a representative example, the ^{1}H NMR spectrum for **1**·BArF is presented in Figure 6; the remaining ^{1}H NMR data are provided in the Supporting Information. The observation that the ^{1}H NMR signals for compounds **1**·BArF, **2**·ClO_4, and **3**·ClO_4 are found in a rather narrow spectral window of 0−22 ppm (as compared to those for monomeric iron(III) porphyrin {range 0−80 ppm}[17,64] and monomeric TMPA−Fe(III) complexes {range 0−250 ppm}[31,47]) and are consistent with the magnetic data (vide supra) suggests antiferromagnetic coupling between the two high-spin, $S = 5/2$ Fe(III) nuclei. Thus, the μ-oxo (O^{2-})-bridged structure, as found in the solid state, is retained in solution. In line with this, the complexes are found to be EPR-silent, overall $S = 0$ spin systems.

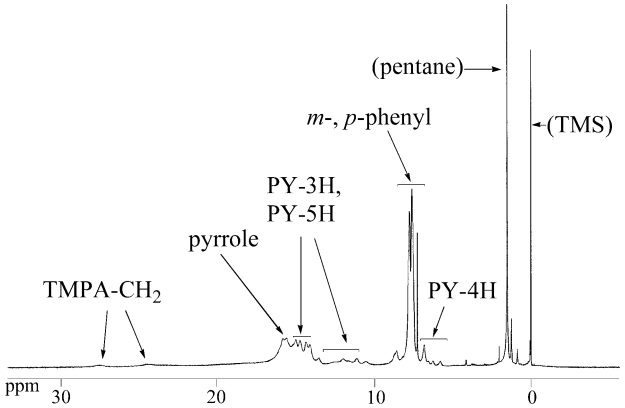

Figure 6. ^{1}H NMR spectrum and probable proton assignments for **1**·BArF.

To properly assign the individual peaks in the ^{1}H NMR spectrum of **1**·BArF, **2**·ClO_4, and **3**·ClO_4, a series of methyl-substituted TMPA compounds were synthesized (Figure 1). The ^{1}H NMR data for the 3-, 4-, and 5-methyl-substituted, self-assembled compounds **6**·ClO_4, **7**-d_8·ClO_4, and **8**-d_8·ClO_4 are presented in Table 5. This allows for the identification of the pyridyl proton 3-, 4-, and 5-positions in **1**·BArF, **2**·ClO_4, and **3**·ClO_4 by correlation to a methyl substituent (or proton peak absence) in **6**·ClO_4, **7**-d_8·ClO_4, and **8**-d_8·ClO_4; the unsubstituted pyridyl positions of course remain unaffected.[44] Although the overall features of tethered and untethered Fe−O−Fe′ spectra are comparable, the spectra for **1**·BArF and **2**·ClO_4 are somewhat different from those for the untethered complexes; the inherent asymmetry of the ligands ^{5}L and ^{6}L gives rise to more complicated spectra.

Indeed, new methyl peaks appear for the substituted complexes, with the concomitant loss of pyridyl proton peaks. The spectra of **1**·BArF, **2**·ClO_4, and **3**·ClO_4 each display peaks that are attributable to the pyridyl portion of the TMPA ligand: 15−10 ppm (3-H and 5-H) and 6.7−6.1 ppm (4-H). These assignments are consistent with the ^{1}H NMR data obtained by Que and co-workers for oxo-bridged (O^{2-}) TMPA(Fe) systems, where the pyridyl 3- and 5-H signals are reported between 11.5 and 17.7 ppm and the pyridyl 4-H signals appear from 6.5 to 7.5 ppm.[31,32] The unmetalated TMPA ligand has pyridyl protons in the diamagnetic region (3-H, δ 7.58; 4-H, δ 7.82; 5-H, δ 7.29), while iron insertion causes a paramagnetic shifting of the pyridyl protons. Both the 3- and 5-pyridyl protons are located four atoms away from the iron center, while the 4-pyridyl proton is located five atoms from the iron.

Whether the paramagnetic shifts are caused by a through-bond or through-space interaction is uncertain. However,

(61) Junk, P. C.; McCool, B. J.; Moubaraki, B.; Murray, K. S.; Spiccia, L.; Cashion, J. D.; Steed, J. W. *J. Chem. Soc., Dalton Trans.* **2002**, 1024−1029.

(62) Helms, J. H.; Haar, L. W. t.; Hatfield, W. E.; Harris, D. L.; Jayaraj, K.; Toney, G. E.; Gold, A.; Mewborn, T. D.; Pemberton, J. R. *Inorg. Chem.* **1986**, *25*, 2334−2337.

(63) Chaudhuri, P.; Winter, M.; Della Védova, B. P. C.; Bill, E.; Trautwein, A.; Gehring, S.; Fleischhauer, P.; Nuber, B.; Weiss, J. *Inorg. Chem.* **1991**, *30*, 2147−2157.

(64) Ghiladi, R. A.; Kretzer, R. M.; Guzei, I.; Rheingold, A. L.; Neuhold, Y.-M.; Hatwell, K. R.; Zuberbüehler, A. D.; Karlin, K. D. *Inorg. Chem.* **2001**, *40*, 5754−5767.

Table 6. ^{2}H NMR Data and Assignments for Compounds **2**-d_2·ClO_4, **2**-d_{10}·ClO_4, **4**·ClO_4, **5**·ClO_4, **6**-d_8·ClO_4, **7**-d_8·ClO_4, and **8**-d_8·ClO_4

assignment	**2**-d_2	**2**-d_{10}	**4**	**5**	**6**	**7**	**8**
$-OCD_2-$	5.84	5.84					
pyrrole-D		15.9			15.28	15.17	15.38
TMPA-6,6′-d_2			19.58, 17.69				
TMPA-CD_2				19.31, 11.56, 4.27			

clearly the 3- and 5-pyridyl protons are closer to the non-heme iron ion, both through bond and through space, relative to the 4-pyridyl proton, and hence, larger paramagnetic downfield shifts are observed. The introduction of methyl substituents in the 3-, 4-, and 5-positions of TMPA did not alter the locations of the pyrrole or the *m*- and *p*-phenyl proton resonances, suggesting that methylation of TMPA has very little effect on the electronics of the porphyrin system. For the free ligands *n*-Me_3TMPA (where $n = 3$, 4, or 5), the peaks for the methyl protons appear near 2.5 ppm in the ^{1}H NMR spectrum for each respective ligand.[44] In the case of complexes **6**−**8**, the methyl peaks are both upfield and downfield paramagnetically shifted (relative to that of the free ligand). The peaks for the methyl groups in the 3- and 5-pyridyl positions are shifted upfield (for 3-Me) and both upfield and downfield (for 5-Me), relative to that of the free ligand, suggesting a predominantly σ-contact shift mechanism. In contrast, the peaks for the methyl groups in the 4-pyridyl positions exhibit only downfield shifts, consistent with a π-contact shift mechanism.[44,65]

Deuterium incorporation into the pyrrole positions for complexes **2**-d_{10}·ClO_4, **6**·ClO_4, **7**-d_8·ClO_4, and **8**-d_8·ClO_4 (Figure 1) allowed for the unambiguous assignment of a pyrrole proton resonance located between 15 and 16 ppm. Table 6 contains ^{2}H NMR data for the pyrrolic deuterium-labeled compounds **2**-d_2·ClO_4, **2**-d_{10}·ClO_4, and **4**−**8**, while spectra are found in the Supporting Information. Typical pentacoordinate, high-spin ferric porphyrin complexes exhibit a pyrrole signal near 80 ppm. The upfield shift of the pyrrole resonances to 15−16 ppm in the Fe−O−Fe′ compounds is attributable to antiferrogmagnetic coupling between $S = 5/2$ iron centers through a bridging oxo (O^{2-}) ligand, leading to a system with little net spin ($S = 0$) and subsequently small paramagnetically shifted signals. Similar coupling is observed in the oxo-bridged complex $[(TPP)Fe]_2O$ ($\delta_{pyrrole} \approx 13.5$ ppm) and in the peroxo-bridged complexes $[(TPP)Fe]_2O_2$ ($\delta_{pyrrole} \approx 16$ ppm)[66] and $[(F_8)Fe]_2O_2$ ($\delta_{pyrrole} \approx 17.5$ ppm).[64]

Using the complex **5**·ClO_4 allowed for the assignment of the $-CD_2-$ methylene protons on the tripodal arms of TMPA (see Table 6). These signals, which are broad and generally unobserved in ^{1}H NMR spectra, are readily detected at 19.31, 11.56, and 4.27 ppm. The latter two signals are generally overlapped by pyridyl and/or solvent peaks; however, the broad resonance near 20 ppm, observed in the ^{1}H NMR spectra for **1**·BArF, **2**·ClO_4, and **3**·ClO_4, can now be definitively assigned to the TMPA $-CH_2-$ protons. In the free TMPA ligand, the methylene $-CH_2-$ protons are found near 3.95 ppm; this methylene spacer, whose methylene protons are located four atoms from the iron centers, shows a considerable paramagnetic shift upon coordination of iron into TMPA, similar to the 3- and 5-pyridyl proton shifts. Labeling of the benzylic, bridging $-OCD_2-$ group in compounds **2**-d_2·ClO_4 and **2**-d_{10}·ClO_4 allows for the assignment of these bridging methylene protons at 5.84 ppm; see Table 6.

A final study involved the selective deuteration of two of the three 6-pyridyl positions of TMPA, in **4**·ClO_4, revealing proton resonances in a 2:1 integration ratio at 19.58 and 17.69 ppm for the 6-pyridyl position of TMPA. This splitting and downfield shifting, compared to a single peak at 8.64 ppm in the free TMPA ligand, arises from two factors: (1) the close proximity of the 6-pyridyl protons to the iron ion in TMPA (three atoms removed), resulting in chemical shift attenuation via a σ-contact shift mechanism, and (2) asymmetry of the tethered ligand and at the iron site. Complexes such as **1** and **2** might exist, in solution, in at least two possible isomeric forms: (1) the chloride ligand *trans* to the tethered pyridyl arm (as seen in the X-ray crystal structure for **2**); (2) the chloride ligand *trans* to an untethered pyridyl arm (as observed in the X-ray crystal structure for **1**).

To summarize, the ^{1}H and ^{2}H NMR data for the related complexes **4**−**8** reveal the most probable assignments for the proton signals observed in the spectra of **1**−**3**. Clearly, the tethered complexes **1** and **2** maintain their intramolecular bridged Fe−O−Fe′ structures in solution.

Summary/Conclusion

The new heme/non-heme diiron complexes **1**·BArF and **1**·PF_6 have been synthesized in good yield from the reaction of the $(^6L)Fe^{II}$ empty tether with an additional equivalent of $FeCl_2$ and counterion, plus dioxygen. The complexes of **1** have been extensively characterized; the X-ray crystal structure of **1**·PF_6 reveals an intramolecular bridging Fe−O−Fe′ moiety that is less bent than those of the previously structurally characterized heme/non-heme compounds **2**·ClO_4 and **3**·ClO_4. Complexes of **1** are further characterized by ^{1}H NMR, resonance Raman, Mössbauer, and UV−vis spectroscopies, MALDI-TOF mass spectrometry, and SQUID magnetic susceptometry. Comparative examination of a series of methyl- and deuterium-substituted untethered Fe−O−Fe′ analogues allowed for the assignment of proton resonances in complexes of **1**−**3**. The Mössbauer spectroscopy and magnetic properties of the untethered compounds **3** and **6** have also been examined for a direct comparison to the tethered species **1** and **2**. Together, these complexes represent spectroscopic models for the putative Fe−O−Fe′ resting active site in NOR; continuing efforts are directed toward the synthesis and characterization of diferrous heme/non-heme complexes to examine their possible biomimetic reactivity with dioxygen and nitric oxide.

(65) Kluiber, R. W.; Horrocks, W. D. *Inorg. Chem.* **1967**, *6*, 1427−1429.
(66) Chin, D.-H.; La Mar, G. N.; Balch, A. L. *J. Am. Chem. Soc.* **1980**, *102*, 4344−4349.

Acknowledgment. This work was supported by National Institutes of Health Grants GM60353 (to K.D.K.) and GM18865 (to P.M.-L.).

Supporting Information Available: Additional ORTEP representations of $[(^6L)Fe-O-Fe(OMe)]PF_6$ (Figures S1 and S2), crystallographic and structural refinement details (Table S1), atomic coordinates and equivalent isotropic displacement parameters (Table S2), complete bond lengths and bond angles (Table S3), anisotropic displacement parameters (Table S4), H-atom coordinates (Table S5), magnetic susceptibility data for **1**·BArF (Figure S3) and **6**·ClO_4 (Figure S4), ^2H NMR data for the representative compounds **4**·ClO_4, **5**·ClO_4, and **6**-d_8·ClO_4 (Figure S5), and ^1H NMR data for **3**·ClO_4 and selected methyl-TMPA-substituted complexes **6**·ClO_4, **7**-d_8·ClO_4, and **8**-d_8·ClO_4 (Figure S6). This material is available free of charge via the Internet at http://pubs/acs.org.

IC0348143